Melt Processing, Mechanical, and Fatigue Crack Propagation Properties of Reactively Compatibilized Blends of Polyamide 6 and Acrylonitrile–Butadiene–Styrene Copolymer

Ulrich A. Handge,[1] Andrzej Galeski,[2] Sung Chul Kim,[3] Dirk J. Dijkstra,[4] Christian Götz,[1] Frank Fischer,[1] Goy Teck Lim,[1] Volker Altstädt,[1] Claus Gabriel,[5] Martin Weber,[5] Helmut Steininger[5]

[1]*Department of Polymer Engineering, Faculty of Engineering Science, University of Bayreuth, Universitätsstrasse 30, 95447 Bayreuth, Germany*
[2]*Center of Molecular and Macromolecular Studies, Polish Academy of Sciences, Sienkiewicza 112, 90363 Lodz, Poland*
[3]*KAIST, 373-1 Guseong-dong, Yuseong-gu, Daejeon 305-701, Korea*
[4]*Bayer MaterialScience AG, CAS-INN-Physics, 51368 Leverkusen, Germany*
[5]*BASF SE, Polymer Research, 67056 Ludwigshafen, Germany*

Received 5 March 2011; accepted 8 June 2011
DOI 10.1002/app.35055
Published online 10 October 2011 in Wiley Online Library (wileyonlinelibrary.com).

ABSTRACT: Within a IUPAC study, melt processing, mechanical, and fatigue crack growth properties of blends of polyamide 6 (PA 6) and poly(acrylonitrile–butadiene–styrene) (ABS) were investigated. We focused on the influence of reactive compatibilization on blend properties using a styrene–acrylonitrile–maleic anhydride random terpolymer (SANMA). Two series of PA 6/ABS blends with 30 wt % PA 6 and 70 wt % PA 6, respectively, were prepared with varying amounts of SANMA. Our experiments revealed that the morphology of the matrix (PA 6 or ABS) strongly affects the blend properties. The viscosity of PA 6/ABS blends monotonically increases with SANMA concentration because of the formation of high-molecular weight graft copolymers. The extrudate swell of the blends was much larger than that of neat PA 6 and ABS and decreased with increasing SANMA concentrations at a constant extrusion pressure. This observation can be explained by the effect of the capillary number. The fracture resistance of these blends, including specific work to break and impact strength, is lower than that of PA 6 or ABS alone, but increases with SANMA concentration. This effect is most strongly pronounced for blends with 70 wt % PA 6. Fatigue crack growth experiments showed that the addition of 1–2 wt % SANMA enhances the resistance against crack propagation for ABS-based blends. The correlation between blend composition, morphology and processing/end-use properties of reactively compatibilized PA 6/ABS blends is discussed. J Appl Polym Sci 124: 740–754, 2012

Key words: polymer blends; reactive compatibilization; maleic anhydride; fatigue crack propagation

INTRODUCTION

A technologically attractive procedure to tailor properties of polymeric materials is blending.[1–4] The main objective of polymer blending is the synergistic combination of advantageous properties of the blend constituents. Because of the low entropy of mixing that is associated with the large molar mass, most pairs of polymers are immiscible (incompatible) and form multiphase polymer blends.[5,6] In general, altering the nature of the interface between different phases by an appropriate compatibilizer enhances mechanical properties of polymer blends. To improve the processability and the performance of polymer blends, it is necessary to have a profound understanding of the physicochemical processes that control melt processing and deformation behavior in the solid state.

Blends of polyamide 6 (PA 6) and acrylonitrile–butadiene–styrene copolymers (ABS) are a commercially important example of multiphase polymer blends.[7] These blends are generally characterized by high impact strength and good chemical resistance in combination with excellent flow properties. In this work, a systematic study of morphological, mechanical, and rheological properties of PA 6/ABS blends was performed to explore the impact of compatibilizer concentration on blend properties using the commercial compatibilizing agent SANMA (a

Correspondence to: U. A. Handge (ulrich.handge@uni-bayreuth.de).
Contract grant sponsor: International Union of Pure and Applied Chemistry; contract grant number: 2005-023-2-400.

TABLE I
Contributions of Different Laboratories to the Investigations of This Work

Institution	Representatives	Contribution
BASF SE (Ludwigshafen, Germany)	C. Gabriel, H. Steininger, M. Weber	Blend preparation, tensile and Charpy tests, and capillary rheometry
Bayer MaterialScience AG (Leverkusen, Germany)	D.J. Dijkstra	Linear viscoelastic shear oscillations
KAIST (Daejeon, South Korea)	S.C. Kim	Transmission electron microscopy (TEM)
Polish Academy of Sciences (Lodz, Poland)	A. Galeski	X-ray scattering (SAXS, WAXS), Izod tests
Polymer Engineering (University of Bayreuth, Germany)	V. Altstädt, F. Fischer, C. Götz, U.A. Handge, G.T. Lim	Fatigue crack propagation experiments, morphological investigations (SEM)

styrene–acrylonitrile–maleic anhydride copolymer). These investigations were carried out in the framework of the IUPAC Subcommittee "Structure and Properties of Commercial Polymers," cf. Table I.

A number of research activities was devoted to reactively compatibilized blends of PA 6 and an ABS copolymer [or a styrene–acrylonitrile copolymer (SAN) for fundamental studies].[8–11] The works of Lee et al.[10] and Takeda and Paul[12] revealed that reactive compatibilization decreases the average size of the dispersed phase, whereby a minimum average size of the dispersed phase exists at a viscosity ratio of 0.75 (viscosity of dispersed phase/viscosity of matrix phase). The influence of the ABS type and the blend composition on the morphological, rheological, and mechanical properties of PA 6/ABS blends reactively compatibilized by an imidized acrylic polymer was the subject of the work of Kudva et al.[11] ABS types with a narrow distribution of rubber particles and a low viscosity in the melt led to a high toughness at low temperatures. The morphology of uncompatibilized and compatibilized blends of PA 6 and styrenic polymers were compared by Majumdar et al.[13] This work elucidated the impact of adding a compatibilizing agent on the evolution of the morphology during extrusion. The size of the dispersed phase strongly decreased in the initial section of the extrusion screw. In subsequent sections of the screw, coalescence of dispersed domains occurred, which must be taken into account for optimization of the blend morphology.

Tensile tests described in Ref. 14 indicate a possible relationship between the size of SAN particles and plastic deformation. The impact strength of PA 6/ABS blends versus compatibilizer concentration of a specific styrene–maleic anhydride copolymer exhibited a maximum that was explained by the high functionality of the compatibilizer.[15] Furthermore, the most efficiently dispersed ABS domains yielded the lowest tough-to-brittle transition temperature.[16] Pressly et al.[17] showed that the concept of the essential work of fracture can be applied to determine the fracture properties of PA 6/ABS blends at different temperatures. Carvalho and coworkers investigated the morphology and impact properties of reactively compatibilized PA 6/ABS blends.[18–20] Blends that were compatibilized using a maleated copolymer were associated with a large impact strength.[19] Microscopic studies of the deformation zone in SAN/rubber blends were performed in Ref. 21. The analysis of the fracture surface in tensile experiments suggested a relaxation at the crack tip induced by local heating at large deformation rates. Recently, micromechanical investigations of thin sections of PA 6/ABS and PA 6/SAN blends under uniaxial loading were performed employing transmission electron microscopy (TEM) equipped with an *in situ* micro tensile stage.[22,23] It was demonstrated that the moisture content of the blends strongly influenced the deformation mechanism. Fibrillation of the interface between ABS/SAN inclusions and the PA 6 matrix and subsequent debonding of ABS or SAN particles were the dominant failure mechanisms in "wet" (conditioned at standard temperature and direct water contact) PA 6/ABS blends.[23] In PA 6/ABS blends with a styrenic matrix (ABS or SAN), crazes were initiated at the poles of elongated PA 6 inclusions. Finally, several authors studied the melt rheology of PA 6/ABS blends in linear viscoelastic shear oscillations,[9] in melt elongation,[24–27] and in a mixed flow using the torque Brabender plastograph.[28] These studies revealed that reactive compatibilization has a strong impact on the viscoelastic properties of PA 6/ABS blends. Furthermore, reactive compatibilization also affects the morphology of the blends and their rheological properties.[8] In these previous works, the flow properties of PA 6/ABS blends were studied at low and moderate deformation rates, whereas polymer processing is mostly associated with large shear and elongational rates.

The objective of this study was to elucidate the influence of reactive compatibilization on melt processing properties and mechanical performances of PA 6/ABS blends. A commercially available random terpolymer containing maleic anhydride groups was

TABLE II
Compilation of Glass Transition Temperature (T_g), Melting Temperature (T_m), Molar Masses (M_n and M_w), and Polydispersity of the Polyamide 6 (PA 6) and the Acrylonitrile–Butadiene–Styrene (ABS) Copolymer Used In This Study

	T_g (°C)	T_m (°C)	M_n (g/mol)	M_w (g/mol)	M_w/M_n
PA 6	52	218	26,000	102,000	3.9
ABS	108	–	36,000	118,000	3.3

The rubber content in the ABS phase was 10.2 wt %.

used as compatibilizer. In contrast to previous works,[24–27] the influence of reactive compatibilization on flow properties at high shear rates and on mechanical properties that are relevant for technical applications was studied. In previous works failure mechanisms in thin sections of PA 6/ABS and PA 6/SAN blends were studied, whereas we here investigate the bulk properties of the blends. Because the microstructure of blends with a co-continuous morphology is complex, we focused on PA 6/ABS blends with a disperse phase formed by either PA 6 or ABS and systematically varied the amount of compatibilizer.

EXPERIMENTAL

Materials and sample preparation

The components of the blends investigated were PA 6 and an ABS copolymer; for details, refer to Table II. All materials were provided by BASF SE (Ludwigshafen am Rhein, Germany). The rubber content in the ABS phase was 10.2 wt %. To compatibilize the interphase between PA 6 and ABS during melt extrusion, a styrene–acrylonitrile–maleic anhydride random terpolymer was added. The terpolymer contained 2 wt % maleic anhydride, 29 wt % acrylonitrile, and 69 wt % styrene. Its number–average molecular mass M_n was 52 000 g/mol, and its weight average molecular mass M_w was 115,000 g/mol. During melt processing, the terminal amino groups of PA 6 react with the maleic anhydride groups of SANMA (see Fig. 1). Two series of blends were prepared. The first series contained 30 wt % PA 6, (70 − x) wt % ABS, and x wt % SANMA, and the second one contained 70 wt % PA 6, (30 − x) wt % ABS, and x wt % SANMA. The weight fraction x of SANMA was set to 0, 1, 2, 4, and 6, respectively. The physical mixture of PA 6, ABS, and SANMA was blended using a twin screw extruder ZSK 30 (Coperion Werner & Pfleiderer GmbH & Co. KG, Stuttgart, Germany, throughput 10 kg/h). The screw rotation rate and the mass temperature were set to 200 revolutions/min and 250°C, respectively. Having been extruded and granulated, the neat blend components and the ten PA 6/ABS blends were injection molded into plates of dimensions 4 mm × 150 mm × 150 mm. The plates were prepared on the Allrounder 420C injection-molding machine (Arburg GmbH & Co. KG, Lossburg, Germany), at a melt temperature of 250°C and a mold temperature of 60°C.

Specimens for mechanical tests were prepared as follows: first, injection-molded plates were dried at 80°C in vacuum (below 1 mbar) whilst shielded from light exposure for 7 days. Second, the dried plates were annealed to essentially remove stress. Annealing was performed in a vacuum press at moderate 225°C for 9 min followed by cooling to 25°C at a rate of 10 K/min. The efficacy of the process was checked by TEM. The criteria chosen were almost complete shape relaxation and no obvious reaggregation of the dispersed phase. Subsequently, samples with a thickness of 3.8 mm were milled out of the annealed plates. Before testing, the specimens were stored at standard climate conditions (23°C, 50% relative humidity) for 14 days.

Cylindrical samples for rheological experiments were also prepared by compression molding of the injection-molded plates. Before molding, the sheets were dried at 80°C for 6 days under vacuum and protection from light. Molding temperature and time were 240°C and 10 min (excluding cooling), respectively. Cylindrical samples for shear rheometry were then milled out of the inner part of the compression-molded plates (dimensions 2 mm × 90 mm × 120 mm), where oxidation of the product was expected to be negligible. Before rheological experiments were started, samples were stored under vacuum for 7 days at 80°C with protection from light. Once removed from the vacuum oven, the sample was immediately placed into the rheometer.

Wide- and small-angle X-ray scattering

A computer-controlled X-ray diffractometer (Philips PW 3830, The Netherlands) was used to acquire 2θ scans of scattered Cu Kα radiation. The sealed-tube X-ray source of the equipment was operated at 50 kV and 30 mA. An angle increment of 0.1° was used for all scans. The rectangular-shaped specimens,

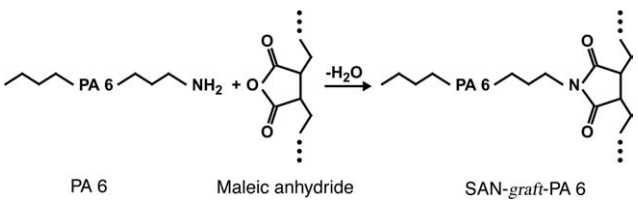

Figure 1 Compatibilizing reaction during melt mixing of polyamide 6 and a terpolymer of styrene–acrylonitrile–maleic anhydride (SANMA). The terminal amino groups of the PA 6 chains react with maleic anhydride groups of SANMA chains and form SAN-*graft*-PA 6 molecules.

about 1 mm thick, were cut out of the core of compression-molded samples (sample preparation for mechanical tests). The scattering contributions from ABS, the amorphous halo of PA 6, and the crystalline peaks of PA 6 were separated mathematically. The computer program WaxsFit (University of Bielsko-Biala, Poland), based on a generic algorithm, was used to deconvolute diffraction profiles. The degree of crystallinity of the PA 6 component of the blends was calculated from the ratio of the integral diffraction peak intensities of PA 6 (crystalline part) to the total scattered intensity from PA 6 originating from the amorphous halo and diffraction peaks.

The lamellar structure of the samples was probed by two-dimensional small angle X-ray scattering (SAXS). A 0.5-m long Kiessing-type camera was equipped with a tapered capillary collimator (XOS) combined with additional pinholes (300 μm in diameter) forming the beam and an imaging plate as a detector medium (Fuji, Tokyo, Japan) The camera was coupled to an X-ray source (sealed-tube, fine point Cu Kα-filtered radiation, operated at 50 kV and 35 mA; Philips, The Netherlands). The acquisition time of the 2D scattering pattern was about 3 h. Exposed imaging plates were read out with a Phosphor Imager SI scanner and ImageQuaNT software (Molecular Dynamics, Sunnyvale, CA). Specimens for SAXS studies were prepared as those for the WAXS investigations. The long period was determined from the angular position of the maximum of the scattered intensity of a background corrected one-dimensional section of the two-dimensional pattern using Bragg's law after background subtraction.

Morphology

Morphological investigations of the compression-molded materials (sample preparation for mechanical tests) were undertaken using TEM. The samples were stained in a 2.0% osmium tetroxide solution for 20 min at room temperature. Thin sections (100–200 nm thick) were cut from the stained materials with a diamond knife at cryogenic conditions (−45°C) using a RMC Powertome XL ultramicrotome. TEM micrographs were made using a JEOL 2000 EX II transmission electron microscope (Jeol, Tokyo, Japan) operated at an acceleration voltage of 100 kV. Osmium-stained rubber particles of ABS appear dark in TEM images. To observe the morphology of PA 6, a supplementary staining step was carried out in which the thin sections already stained with osmium tetroxide were additionally stained in a 3.0% phosphotungstic acid solution at the same conditions. Thereafter, PA 6 also appears dark in TEM micrographs.

Fracture surfaces of samples that failed in fatigue crack growth experiments were inspected by scanning electron microscopy (SEM). The samples had been sputter-coated with a fine-grained layer (∼ 1 nm thick) of platinum using a Cressington Sputter Coater 108 in its automatic mode. SEM digital images were taken at various magnifications using a FE–SEM Leo 1530 FE (Carl Zeiss, Oberkochen, Germany, equipped with a field emission cathode). The acceleration voltage was 3 kV.

Shear rheology

The rheological properties of the neat components and the blends were determined at 240°C. Linear viscoelastic shear oscillations were performed using the ARES rotational rheometer (Rheometric Scientific, Piscataway, NJ) with a nitrogen inert gas atmosphere. A plate–plate geometry with a plate diameter of 25 mm was used. The melting time of the sample was 10 min. The shear amplitude γ_0 was chosen to be 3%, and the gap set to 1.4 mm.

Capillary measurements to determine the apparent viscosity η_{app} were performed using a Rheograph 2003 (Göttfert, Buchen, Germany) at 240°C. The length to radius ratio of the die was 60, and the radius of the die was 0.5 mm. Before testing, the granules of the neat components and the blends were dried *in vacuo* at 80°C for at least 5 days while protected from light. The heating time for melting the pellets was 5 min.

The extrudate swell was determined with a Lasermike (Göttfert, Buchen, Germany). The length to radius ratio of the die was 7.62 and its radius 1.05 mm. To prevent the strand from sagging, it was cut off 1 cm below the optical path of the Lasermike before each measurement. The extrudate diameter d was recorded as a function of pressure.

Mechanical properties

Tensile tests were carried out according to ISO 527-1 using dumbbell like specimens (ISO 527-2/1BA). The conditioning of the specimens was performed as described in the Section "Materials and sample preparation." The Young's modulus was determined at a crosshead velocity of 1 mm/min and all additional quantities (yield stress, maximum stress, and elongation at break) at 5 mm/min.

Impact strength

The impact strength of the neat components and the blends was investigated by means of Charpy (ISO 179-1 and ISO 179-2) and Izod (ISO 180/1 A) tests carried out at standard climate. The tests were performed on notched and unnotched specimens of type ISO 179-1/1eU and type ISO 179-1/1eA, respectively, using a Resil 5.5 instrumented CEAST

TABLE III
Composition of the PA 6/ABS Blends, Degree of Crystallinity, and Long Period of the Lamellae as Determined by WAXS and SAXS, Respectively

Material	PA 6 (wt %)	SANMA (wt %)	SAN (wt %)	PBu-*g*-SAN (wt %)	Degree of crystallinity (%)	Long period (Å)
PA 6	100	0	0	0	31.8	92.6
ABS	0	0	89.80	10.20	–	–
30% PA 6–0% SANMA	30	0	62.85	7.15	30.6	91.7
30% PA 6–1% SANMA	30	1	61.85	7.15	30.6	93.0
30% PA 6–2% SANMA	30	2	60.85	7.15	30.0	91.0
30% PA 6–4% SANMA	30	4	58.85	7.15	30.9	96.6
30% PA 6–6% SANMA	30	6	56.85	7.15	31.1	93.4
70% PA 6–0% SANMA	70	0	26.94	3.06	30.4	92.2
70% PA 6–1% SANMA	70	1	25.94	3.06	30.0	94.3
70% PA 6–2% SANMA	70	2	24.94	3.06	31.5	94.3
70% PA 6–4% SANMA	70	4	22.94	3.06	33.0	94.3
70% PA 6–6% SANMA	70	6	20.94	3.06	30.6	96.4

pendulum impact tester. The impact velocity and energy of the hammer were 3.7 m/s and 5 J, respectively.

Fatigue crack propagation

The resistance of the materials against stable crack propagation under cyclic loading conditions was investigated according to the ESIS TC4 protocol for fatigue crack growth of polymers.[29,30] Compact tension specimens according to ASTM standard E 647 with a ligament length W of 33 mm were cut out of compression-molded plates using a water-cooled saw. The thickness of the samples was 3.8 mm. For each specimen, a sharp precrack ahead of the machined notch was applied by tapping a razor blade into the material. The specimens were conditioned according to the conditions specified in the section "Materials and Sample Preparation."

The initial precrack length a_0 was estimated from the crack depth visible at both sides of the specimen. The dynamic elastic modulus E_{dyn} of the specimen was calculated from a_0, specimen dimensions, and the measured dynamic specimen compliance. The initial value of E_{dyn} is required to calculate the current crack length a as a function of the number of applied load cycles N, see Ref. 31 for details. The fatigue test was started having extended the initial precrack by about 2 mm under computer control by increasing the load amplitude in order to create a natural crack tip.

Dynamic loading of the specimens was performed on a servohydraulic testing machine (Schenck, IST 8800) at room temperature. A Plexiglas plate was mounted in front of the measurement chamber of the testing machine in order to improve the stability of temperature and humidity. The frequency was set to 10 Hz, and the crack opening displacement was monitored using a displacement gauge (MTS 632.13F-20) mounted at the front face. The load was sinusoidally applied in intervals with a constant stress amplitude ΔK. First, the stress amplitude ΔK of each interval was incrementally increased in order to initiate crack propagation. Then, the stress amplitude was continuously decreased to determine the threshold value ΔK_{th} for crack growth. Subsequently, the stress amplitude ΔK was increased at intervals of constant ΔK each time when the crack propagation rate, da/dN, leveled out. da/dN was recorded as a function of ΔK. During the entire test, the load ratio, $R = \sigma_{min}/\sigma_{max}$, was 0.1.

RESULTS

Microstructure

Information about amorphous and crystalline structures of polymers is obtained from X-ray scattering experiments. Table III lists the results of WAXS and SAXS measurements of the neat components and PA 6/ABS blends. Obviously, neither the degree of crystallinity of PA 6 nor its long period is significantly influenced by the amount of ABS (0, 30, and 70 wt %) in the blend or the concentration of the additive SANMA (1–6 wt %), that is, the crystalline structure of PA 6 is not affected by ABS and/or SANMA.

The morphology of the compression-molded blends was analyzed employing TEM. Figure 2(a) depicts the morphology of the neat ABS. Two types of rubber particles are visible—numerous small ones that are fairly well distributed and some larger ones. The morphology of the blends with an ABS matrix (30 wt % PA 6) is presented in Figure 2(b–d). The dark PA 6 inclusions in the ABS matrix are partially debonded and deformed into an elliptical shape due to microtoming. The average size of the PA 6 inclusions decreases with the increase in SANMA concentration. A closer look at the PA 6 inclusions reveals that small, obviously highly compatibilized SAN droplets (micelle-like structures) are embedded

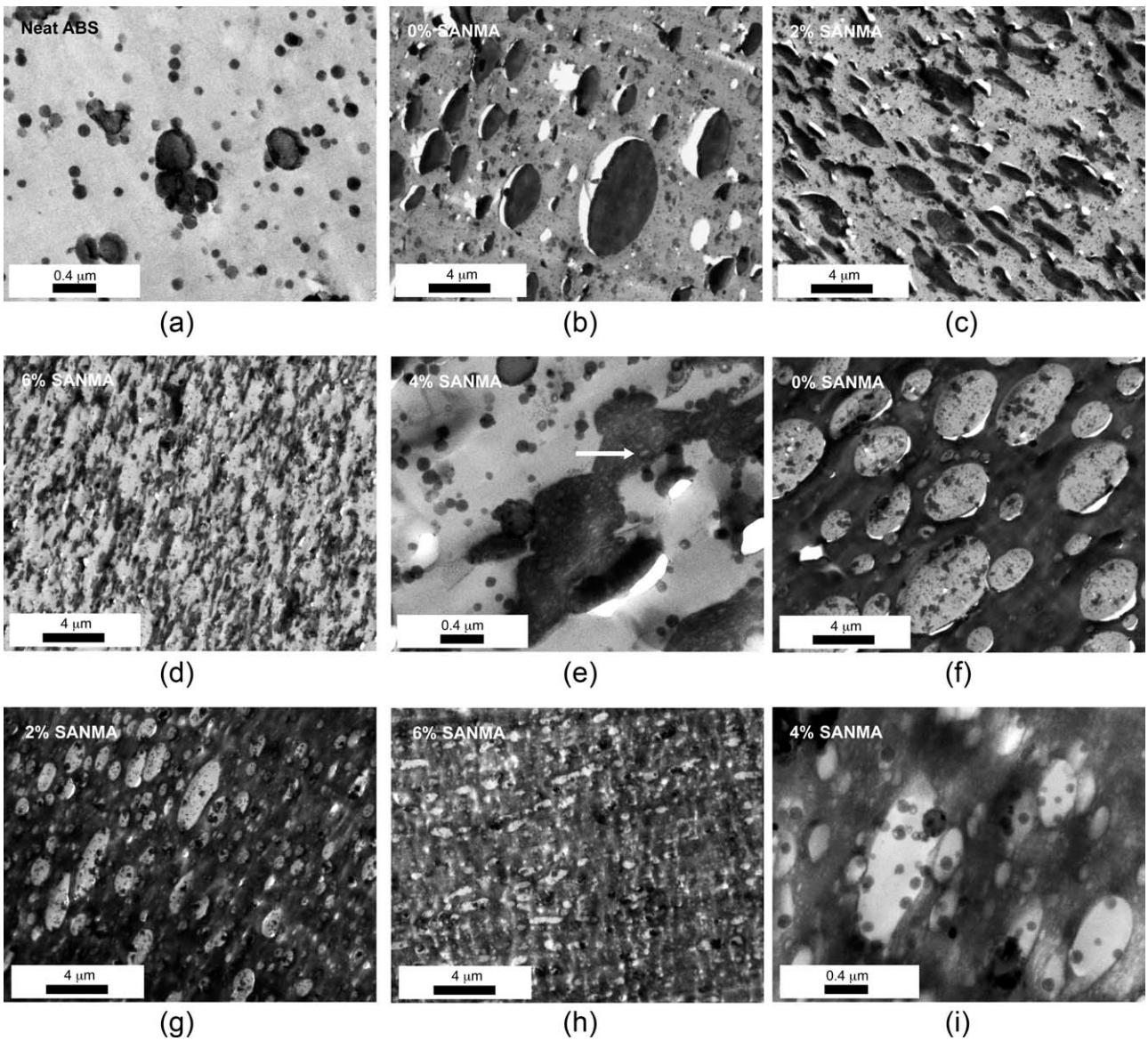

Figure 2 Transmission electron micrographs (TEM) of neat ABS and the PA 6/ABS blends after compression molding. (a) Neat ABS copolymer. (b–e) TEM of 30% PA 6/70% ABS blends. (f–i) TEM of 70% PA 6/30% ABS blends. The concentration of SANMA is indicated.

therein. One of these tiny SAN inclusions is marked by an arrow in Figure 2(e). At large SANMA concentrations (4 and 6 wt %), the shape of the PA 6 inclusions becomes more and more irregular as it has also been reported for related blends.[26]

Figure 2(f–i) presents the morphology of the blends with a PA 6 matrix (70 wt % PA 6/30 wt % ABS). The micrographs reveal that the ABS component forms a large number of ellipsoidal inclusions that are uniformly dispersed in the PA 6 matrix. Its shape has to be considered again as an artifact arising from microtoming (see above). Similar to the blends with 30 wt % PA 6, the average domain size decreases with the increase in SANMA concentration.

Rheological properties

The absolute value of the complex viscosity η^* as a function of ω and the steady-state apparent viscosity η_{app} versus the apparent shear rate $\dot{\gamma}_{app}$ at 240 °C are presented in Figure 3. These data (without Bagley and Rabinowitsch–Weissenberg corrections) reveal that the relation $|\eta^*(\omega)| = \eta_{app}(\dot{\gamma}_{app})$ with $\omega = \dot{\gamma}_{app}$ seems to be fulfilled for the neat components and the blends. The Newtonian plateau appears for neat PA 6 at low frequencies ω, whereas ABS and the blends do not behave like Newtonian fluids at low ω. For detailed discussions of this effect, the reader is referred to Refs. 32 and 24–27. In particular, the blend with 70 wt % PA 6 and 6 wt %

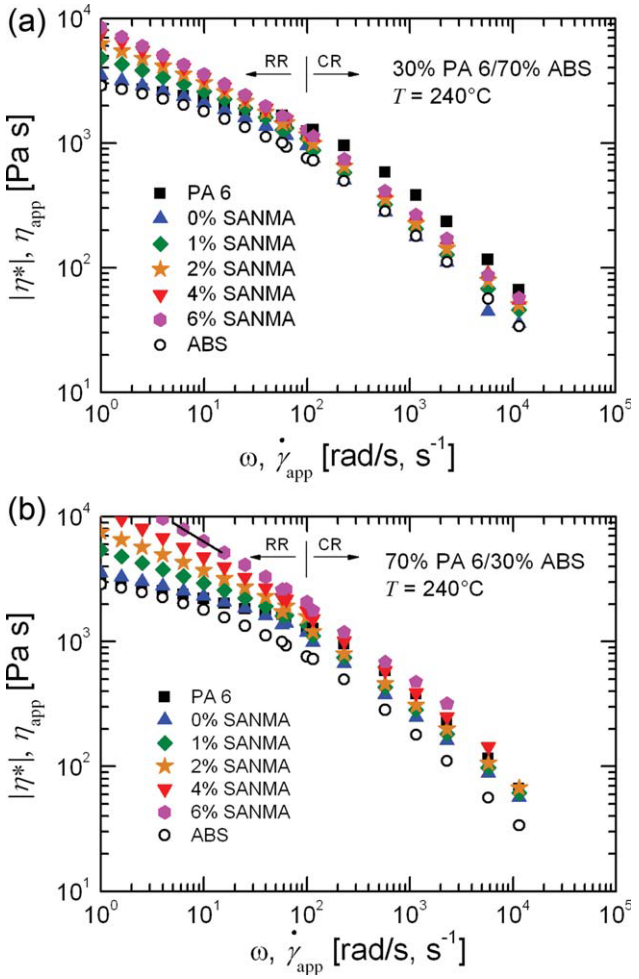

Figure 3 Apparent shear viscosity η_{app} and absolute value of complex viscosity $|\eta^*|$ as a function of apparent shear rate $\dot{\gamma}_{app}$ and frequency ω, respectively, for (a) the neat blend components and the 30% PA 6/70% ABS blends and (b) the neat blend components and the 70% PA 6/30% ABS blends. The test temperature was 240°C. The concentration of SANMA is indicated. The solid line in (b) has a slope of −0.5. The abbreviation "RR" denotes measurements by means of rotational rheometry and "CR" by means of capillary rheometry. [Color figure can be viewed in the online issue, which is available at wileyonlinelibrary.com.]

SANMA shows the behavior of the critical gel state, that is, $|\eta^*| \propto \omega^{-0.5}$ (because of $G' \propto G'' \propto \omega^{0.5}$). This behavior is attributed to the large number of tiny highly compatibilized SAN inclusions in the PA 6 matrix, which increase the elastic interactions between the different domains.[27]

Figure 3(a) shows the viscosity functions of PA 6, ABS, and the five different 30% PA 6/70% ABS blends. Common to all pristine polymers and the various blends is the occurrence of shear thinning. The shear viscosities of the 30% PA 6/70% ABS blends range between those of PA 6 and ABS, and they increase monotonically with SANMA concentrations. The monotonic increase in viscosity expresses the formation of high-molecular weight polymer chains due to grafting of PA 6 onto SANMA molecules. The viscosity functions, η_{app} ($\dot{\gamma}_{app}$), of PA 6, ABS, and the 70% PA 6/30% ABS blends are depicted in Figure 3(b). The shear viscosity of the 70% PA 6/30% ABS blends also increases monotonically with rising SANMA concentrations. However, in contrast to the 30% PA 6/70% ABS blends, the apparent shear viscosity of the 70% PA 6/30% ABS blends containing 4% and 6% SANMA exceeds the viscosity of pure PA 6. This effect is caused by the tiny, highly compatibilized ABS/SAN domains in the PA 6 matrix. Similar results were obtained using torque measurements.[28]

Squeezing a polymer melt through a die causes the coils to deform, and the melt will show an entropy-elastic response (i.e., extrudate swell) at the exit of the die by recoiling of polymer chains. The extrudate swell is defined by the ratio

$$\delta_{extrudate} = d/d_0, \tag{1}$$

where d_0 and d denote the diameters of the die and the extruded strand, respectively. This quantity is a measure of elasticity of a polymer melt. Because the extrudate swell depends on the elongational stress acting before the die and the shear stress along the die, it is determined, among other quantities, by the pressure gradient Δp along the length of the die. Neglecting the Bagley correction, the pressure drop Δp across the die is related to the apparent wall shear stress τ by

$$\tau = d_0 \Delta p/(4L), \tag{2}$$

where L is the length of the die. In multiphase polymer blends, the recoverable deformation is also affected by the interfacial tension between distinct phases. The interfacial tension contributes to the elasticity of the melt and increases the recoverable deformation.[33–35]

The extrudate swell of the two uncompatibilized blends (0% SANMA) was outside the range of measurement. The extrudate swell of neat PA 6 and ABS increases with the pressure drop Δp (see Fig. 4). The value $\delta_{extrudate}$ of all blends is greater than the extrudate swell of the neat components because of the contribution of the interfacial tension between PA 6 and ABS. Furthermore, the extrudate swell decreases with increasing SANMA concentration for both series of blends. A possible explanation of this phenomenon draws on the morphological investigations (see Fig. 2). The average size of the domains obviously decreases with increasing SANMA concentrations. In shear and elongational flows, the stretch

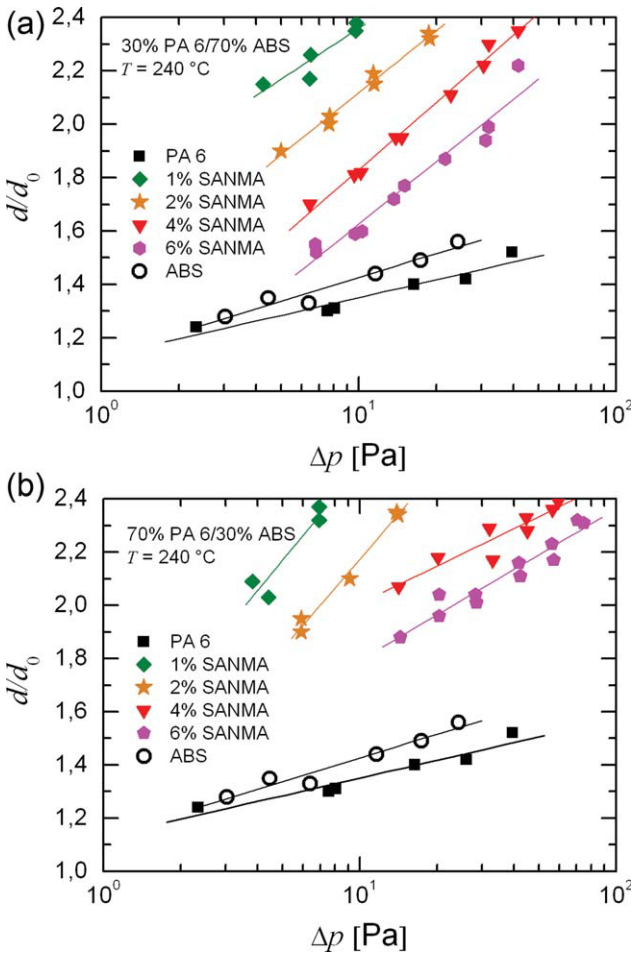

Figure 4 Extrudate swell d/d_0 [see eq. (1)] at 240°C for (a) the neat blend components and the 30% PA 6/70% ABS blends and (b) the neat blend components and the 70% PA 6/30% ABS blends. The radius $d_0/2$ of the die was 1.05 mm and the length-to-radius ratio of the die 7.62. The SANMA concentration is indicated. [Color figure can be viewed in the online issue, which is available at wileyonlinelibrary.com.]

ratio of a drop in a continuous phase increases if the capillary number

$$\mathrm{Ca} = \eta\dot{\gamma}r/\Gamma \tag{3}$$

increases. Equation (3) draws upon the assumption of an isolated drop of radius r in an infinite matrix of viscosity η exposed to a shear rate $\dot{\gamma}$. The interfacial tension between the droplet and the matrix is denoted by Γ. Consequently, smaller droplets are less stretched than larger ones. Hence for the same pressure difference Δp, that is, for the same shear stress τ, cf. eq. (2) the domains of the blends with a larger SANMA concentration are less stretched than the ones with a smaller SANMA concentration.[26] Because a smaller stretch ratio leads to a smaller recoverable deformation, see Ref. 34, the extrudate swell of the PA 6/ABS blends also decreases with increasing concentrations of the compatibilizer. Similar results were obtained in creep experiments in the elongational mode.[36,37] We emphasize that the tiny highly compatibilized ABS/SAN domains in the blends with a PA 6 matrix influence the viscoelastic properties of the blends. They contribute to an increase of viscosity and also influence the recoverable deformation, see Refs. 26 and 27. However, the contribution of the interfacial tension driven to the elastic recovery has been clearly shown in Ref. 26.

Mechanical properties

The mechanical properties of the materials investigated are presented in Figures 5–8 and in Table IV. Figure 5 depicts the nominal stress–strain diagram of the parent components and the blends. PA 6 shows a yield point where the sample begins to neck. As long as it is deformed by cold drawing, the nominal stress remains constant. The average value of the elongation at break of PA 6 is about 216%.

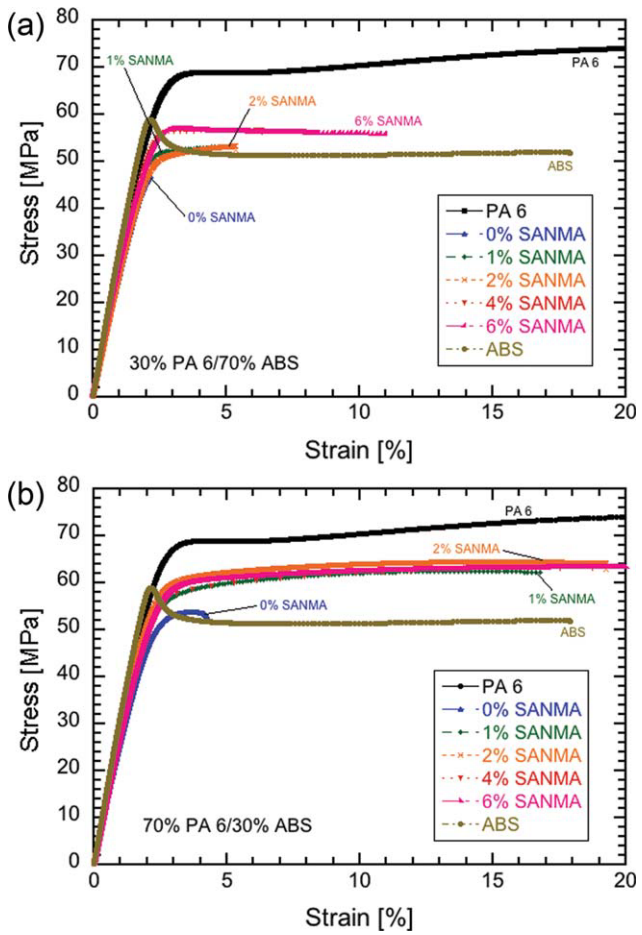

Figure 5 Tensile stress–strain diagram for the neat blend components and (a) the 30% PA 6/70% ABS blends and (b) the 70% PA 6/30% ABS blends with different concentrations of SANMA at room temperature. [Color figure can be viewed in the online issue, which is available at wileyonlinelibrary.com.]

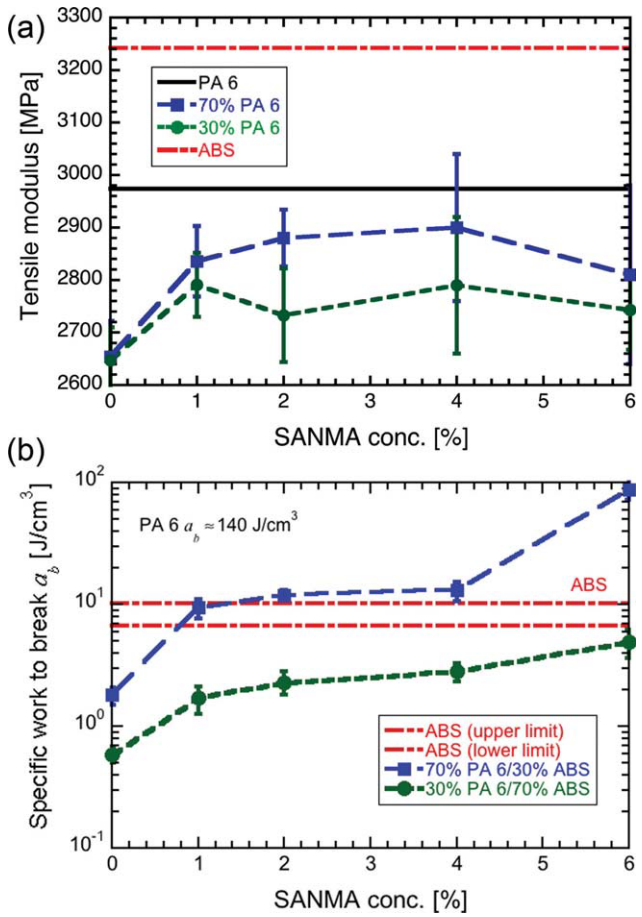

Figure 6 Mechanical properties of the neat components and the blends investigated. (a) Tensile modulus E and (b) specific work to break a_b of compression-molded samples. [Color figure can be viewed in the online issue, which is available at wileyonlinelibrary.com.]

ABS shows stress-whitening. It deforms at almost constant cross section and fails at about 18% of strain. The 30% PA 6/70% ABS blend with 0% SANMA behaves in a very brittle manner. With increasing amounts of compatibilizer, the elongation at break of the 30% PA 6/70% ABS blends increases from some 2.2% (for 0% SANMA) to 11.2% (for 6% SANMA) and stress-whitening develops again. In the strain interval of plastic deformation (i.e., at strains above $\sim$ 3%), the tensile stress level of the 30% PA 6/70% ABS blend with 6% SANMA ranges between that of the pristine components, roughly following a rule of mixture. In contrast to neat ABS and neat PA 6, compatibilized blends do not display a distinct yield point. Like the blend with 30% PA 6 and 0% SANMA, the uncompatibilized 70% PA 6/30% ABS blend is a brittle material. With increasing SANMA concentrations, the elongation at break increase from 4.5% (for 0% SANMA) to 151% (for 6% SANMA). 70% PA 6/30% ABS blends with 4% of SANMA neck during tensile deformation like neat PA 6 and additionally show stress-whitening. Above strains of 3% the tensile stresses of the compatibilized blends also range between the values of pristine ABS and PA 6.

The modulus of elasticity E and the specific work to break of the neat components and of the two different blend series are plotted versus SANMA concentration in Figure 6. The analysis of the data yields $E = 2974$ MPa for neat PA 6 and $E = 3242$ MPa for neat ABS. The Young's modulus of the 30% PA 6/70% ABS blend and the 70% PA 6/30% ABS blend with 0% SANMA is clearly below the modulus of the neat components. A moderate increase of tensile modulus is observed by compatibilization with 1% SANMA. Larger concentrations of SANMA do not (blends with 70% PA 6) or only moderately (blends with 70% ABS) affect the modulus. In contrast to the modulus of elasticity, the specific work to break is influenced much more by SANMA. The specific work-to-break values continuously increase with the

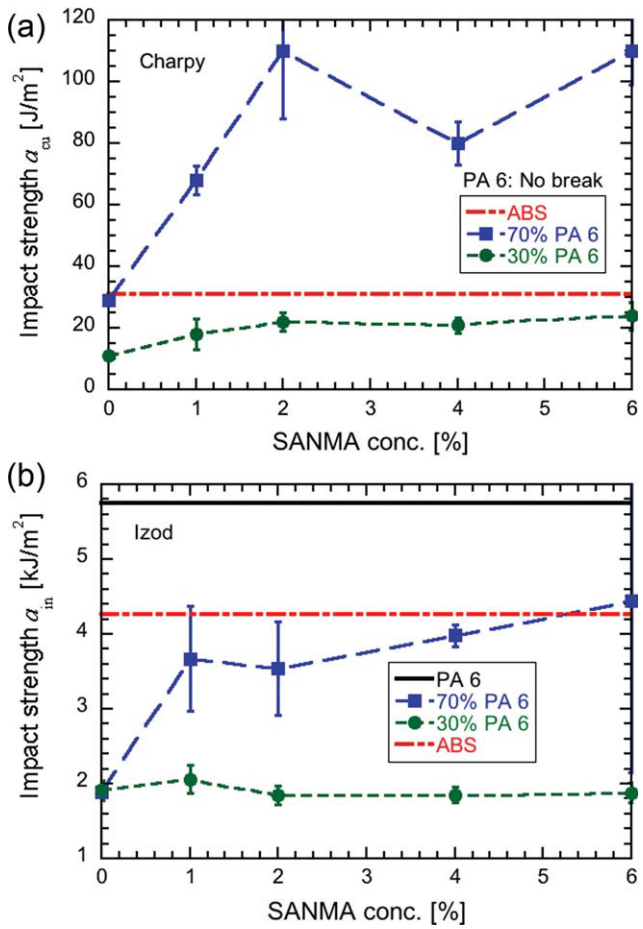

Figure 7 (a) Charpy (unnotched) and (b) Izod (notched) impact strength of two series of PA 6/ABS blends of complimentary composition as a function of SANMA concentration at room temperature. The lines denote the value of neat polyamide 6 (dashed) and of neat acrylonitrile-butadiene-styrene-copolymer (solid). [Color figure can be viewed in the online issue, which is available at wileyonlinelibrary.com.]

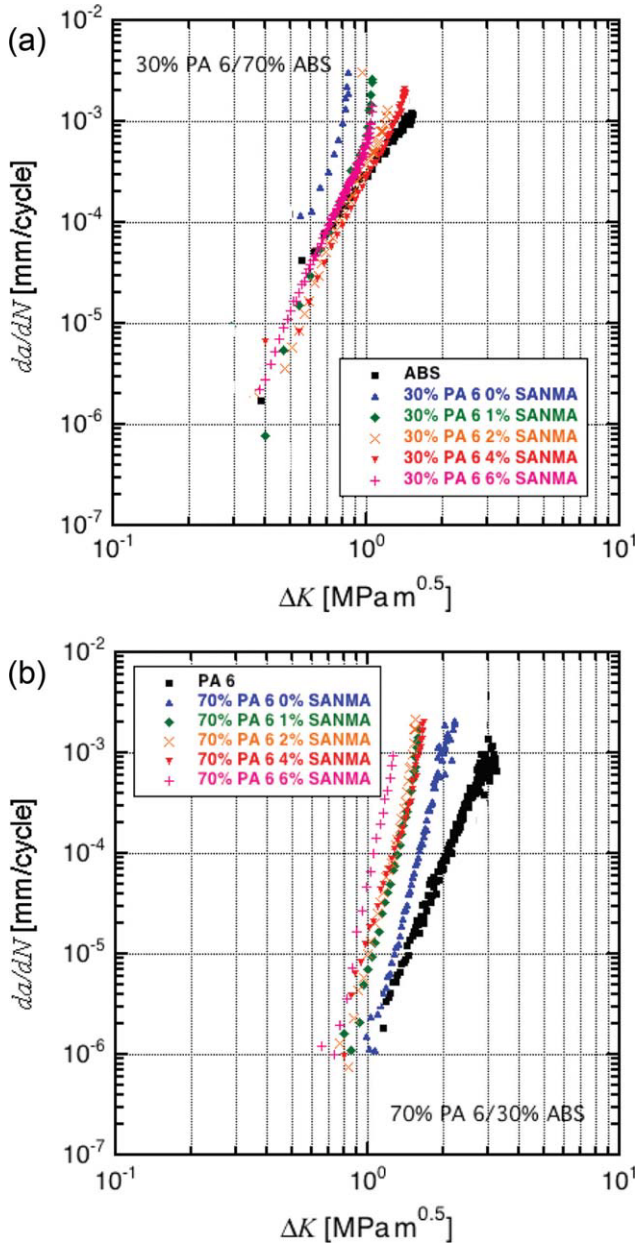

Figure 8 Crack propagation per cycle da/dN versus stress intensity factor difference ΔK at fatigue loading (room temperature, 10 Hz): (a) Neat ABS and 30% PA 6/70% ABS blends and (b) Neat PA 6 and 70% PA 6/30% ABS blends. The concentration of SANMA is indicated. [Color figure can be viewed in the online issue, which is available at wileyonlinelibrary.com.]

compatibilizer concentration and particularly steeply for blends with a continuous PA 6 phase.

The toughness of the various blends was characterized by their notched Izod, a_{in}, and unnotched Charpy, a_{cu}, impact strength (Fig. 7). For both series of blends, the toughness generally increases with SANMA concentration (except for the blend with 70% PA 6 and 4% SANMA); however, it generally stays below that of the parent polymer. The lower toughness of the blends is deemed to be associated with interfacial failure. Charpy and Izod impact strengths of ABS blends do not vary much with SANMA concentrations, whereas the impact strength of the blends with a PA 6 matrix significantly increases with SANMA concentration by roughly a factor of two.

Fatigue crack propagation experiments probe the resistance of a material against crack growth at dynamic loading. Figure 8 shows the crack propagation per cycle da/dN versus the difference of the stress intensity factor $\Delta K = K(F_{max}) - K(F_{min})$. Here, a denotes the length of the crack, N the number of cycles, and F_{min} and F_{max} the minimum and maximum load applied. The stress intensity factor $K(F)$ was calculated from

$$K(F) = \frac{F}{d\sqrt{W}} Y(a/W), \tag{4}$$

where W is the width of the ligament ($W = 33$ mm) and d its thickness ($d = 3.8$ mm). The function $Y(a/W)$ accounts for the geometry of the specimen. The data for neat PA 6 reveal that the crack starts to propagate when the stress intensity factor is above a certain threshold value ΔK_{th}. Stress intensity factors below the threshold value are assigned to the subcritical regime where the crack propagation rate approaches to zero. In the regime of stable crack growth, referred to as the Paris regime, the crack growth rate is associated with the stress intensity factor by the Paris–Erdogan equation[38]

$$da/dN = C(\Delta K)^m, \tag{5}$$

where C and m are material-dependent constants. Figure 8 clearly shows the power-law regime with m equal to 5.8 for PA 6. At very large ΔK values, crack propagation becomes unstable, and the specimen fails rapidly as in static tests (unstable regime).

Neat ABS exhibits a fatigue behavior with a much lower resistance against crack propagation than neat PA 6. The crack propagation rate of neat ABS also increases with ΔK, but with a lower slope ($m = 3.4$). Note that mainly the stable regime can be seen in Figure 8. The noncompatibilized blend with 30% PA 6 and 70% ABS has a lower resistance against crack propagation than the neat matrix material ABS. The resistance against crack propagation of the blends with an ABS matrix increases with SANMA concentrations up to 2% SANMA, but decreases for higher SANMA concentrations. Such a nonmonotonic behavior has also been observed for compatibilized blends of PPE and SAN.[39] Because the size of the plastic zone increases with ΔK and the size of PA 6 inclusions decreases with SANMA concentration, at higher SANMA concentrations, more PA 6 particles are located within the plastic zone in front of the

TABLE IV
Summary of Mechanical Properties of Parent Polymers and the PA 6/ABS Blends Investigated

Material	Young's modulus (MPa)	Yield stress (MPa)	Maximum stress (MPa)	Elongation at break (%)	Fracture toughness (J/cm^3)	Deformation characteristics
PA 6	2974 ± 58	66.6 ± 1.5	79.0 ± 2.1	216.0 ± 18.0	142.0 ± 13.0	Necking
ABS	3242 ± 67	60.6 ± 2.0	60.6 ± 2.0	18.3 ± 3.0	8.5 ± 1.8	Stress whitening
30% PA 6–0% SANMA	2647 ± 63	–	47.3 ± 1.1	2.2 ± 0.2	0.6 ± 0.1	Brittle
30% PA 6–1% SANMA	2791 ± 61	–	53.3 ± 0.9	4.5 ± 0.5	1.7 ± 0.4	Moderate stress whitening
30% PA 6–2% SANMA	2733 ± 89	–	53.8 ± 1.0	5.4 ± 0.9	2.3 ± 0.5	Moderate stress whitening
30% PA 6–4% SANMA	2790 ± 130	56.6 ± 0.3	55.3 ± 1.3	6.2 ± 0.8	2.8 ± 0.5	Moderate stress whitening
30% PA 6–6% SANMA	2743 ± 76	55.9 ± 1.4	55.8 ± 1.4	11.2 ± 1.2	4.9 ± 1.3	Stress whitening
70% PA 6–0% SANMA	2654 ± 68	53.5 ± 1.0	53.0 ± 0.9	4.5 ± 0.6	1.8 ± 0.3	Brittle
70% PA 6–1% SANMA	2836 ± 67	62.2 ± 0.9	62.1 ± 1.0	16.6 ± 2.6	9.4 ± 1.7	Stress whitening
70% PA 6–2% SANMA	2880 ± 54	64.5 ± 0.6	64.5 ± 0.6	20.7 ± 1.8	12.0 ± 1.0	Stress whitening
70% PA 6–4% SANMA	2900 ± 140	64.8 ± 1.5	64.8 ± 1.5	21.8 ± 3.1	13.0 ± 2.3	Stress whitening
70% PA 6–6% SANMA	2810 ± 170	62.6 ± 2.2	65.3 ± 3.4	151.0 ± 22.0	88.0 ± 16.0	Stress whitening and necking

crack tip. The crack propagation resistance of the blends with 70% PA 6 is greater than the resistance of the blends with 30% PA 6. This result indicates that the matrix strongly influences the crack propagation resistance. The resistance of the blends with 70% PA 6 ranges between the corresponding values of neat PA 6 and neat ABS and surprisingly decreases with larger SANMA concentration. Furthermore, the data in Figure 8 show that the crack propagation behavior, that is, the value of m, remains unchanged within the ABS-based and PA 6-based blends and is not affected by the SANMA concentration.

Fracture surfaces of samples having passed the fatigue crack growth experiments were investigated using SEM (see Fig. 9). The micrographs correspond to the regime of stable crack growth. The fracture surface of neat PA 6 is shown in Figure 9(a) and depicts an uneven crack surface indicating ductile failure. Large lamellar fibrils are visible, which are typical for polyamide specimens.[40,41] Figure 9(b) displays the fracture surface of ABS, which is typical for rubber toughened crazing polymers. The roughness of the surface is due to plastically deformed rubber particles and ruptured craze fibrils in the matrix polymer.[42] The holes seen in the micrograph have their origin in voids created by cavitation of rubber particles and their subsequent expansion as the matrix yields. This special grade of neat ABS is quite brittle, because its concentration of rubber particles is only 10 wt %. Figure 9(c) shows the fracture surface of the 30% PA 6/70% ABS blend (not compatibilized). In uncompatibilized blends, the minority component forms spherical particles that are some micrometers in size. In the fracture surface, these particles appear detached from the matrix and are surrounded by voids. The micrograph also reveals that the PA 6 inclusions are only marginally deformed, because weak adhesion to the matrix does not allow for significant stress transfer. Hence, the crack runs entirely through the matrix leaving all debonded particles undeformed. The ABS matrix deforms plastically via shear deformation. Figure 9(d,e) presents the fracture surface of compatibilized 30% PA 6/70% ABS blends. Plastic deformation of the ABS matrix is more pronounced with increasing SANMA concentration. Furthermore, the PA 6 inclusions are deformed more strongly because of improved adhesion between matrix and inclusions. However, the brittle ABS matrix and a still considerable amount of interfacial failure lead to very unfavorable toughness properties at quasi-static, impact, and fatigue loading conditions (cf. Fig. 5–8). A hedgehog pattern seen in Figure 9(h) results from the formation of crazes in the SAN matrix of ABS. The craze fibrils for the pristine ABS and the 70% PA 6/30% ABS blend with 4% SANMA are shown at a higher magnification in Figure 10(a,b). The impact of small quantities of compatibilizer added to the blend, which had already become apparent on mechanical performance and on phase morphologies of the two blends, is clearly evident in SEM images of fracture surfaces. Although without compatibilizer, two phases are easy to distinguish by debonded particles, one now sees a homogeneously deformed surface structure, which is caused by the capability of dispersed particles to adhere to the matrix and to deform plastically with the matrix prior to interfacial failure [Fig. 9(d,e)]. With increasing amounts of SANMA, the average size of PA 6 domains decreases and having been loaded their plastic deformation increases [Fig. 10(c)]. Nevertheless, numerous voids still indicate that the crack has to pass predominantly through the ABS matrix. This phenomenon was observed for all blends with an ABS matrix.

The ABS particles in the uncompatibilized 70% PA 6/30% ABS blend are only marginally deformed, which shows that the fatigue properties are determined by interfacial failure and subsequent plastic

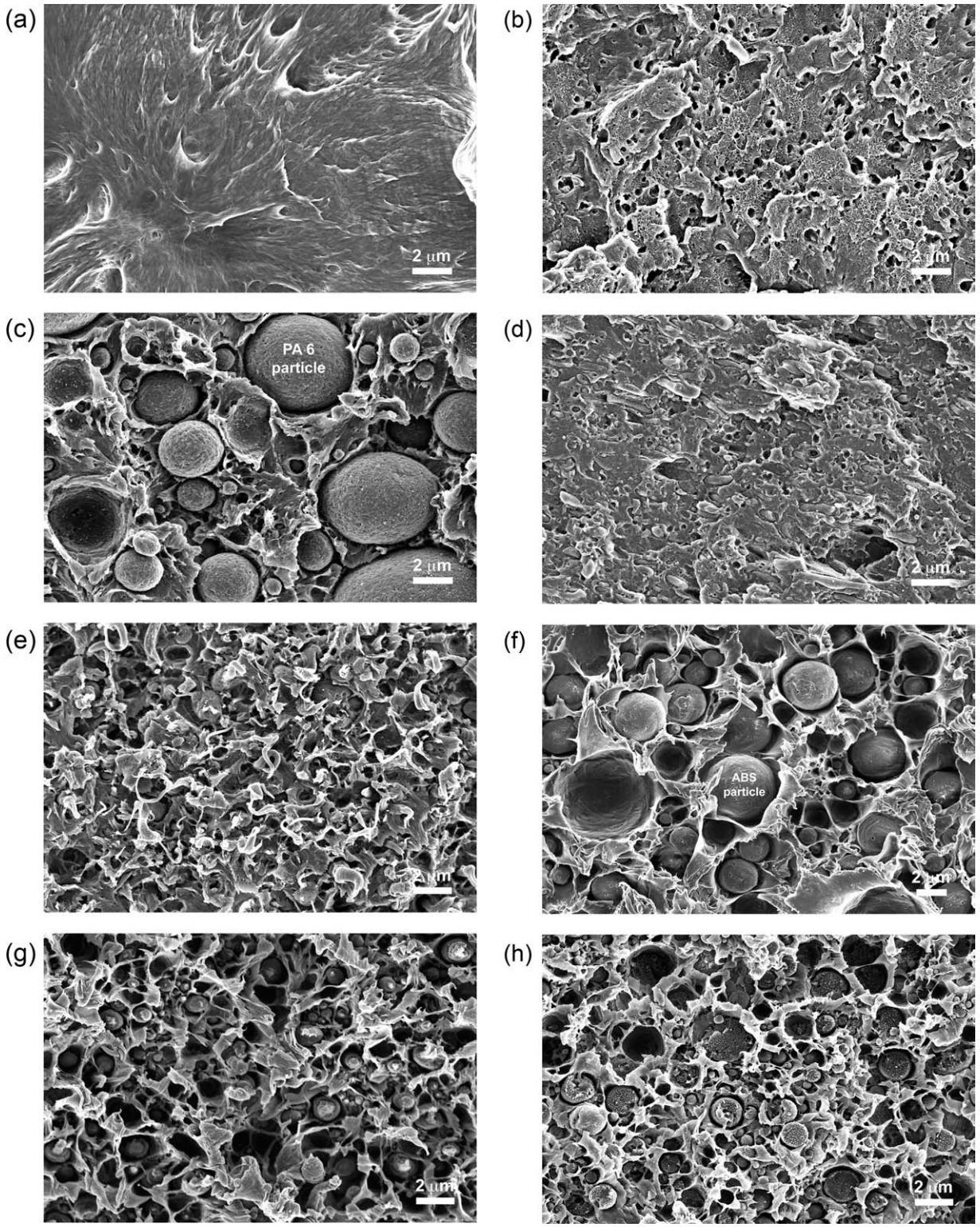

Figure 9 Scanning electron micrographs of the fracture surface of PA 6, ABS, and the PA 6/ABS blends, which were used for the fatigue crack propagation experiments. (a) Neat polyamide 6. (b) Neat ABS copolymer. (c–h) PA 6/ABS blends. The blend composition is (c) 30% PA 6/70% ABS with 0% SANMA. (d) 30% PA 6/70% ABS with 2% SANMA. (e) 30% PA 6/70% ABS with 4% SANMA. (f) 70% PA 6/30% ABS with 0% SANMA. (g) 70% PA 6/30% ABS with 2% SANMA. (h) 70% PA 6/30% ABS with 4% SANMA. The hedgehog like structure observed in the surface of ruptured ABS particles [Fig. 9(h)] is due to crazing. Crazing is initiated when bonding of the particles to the matrix is sufficient.

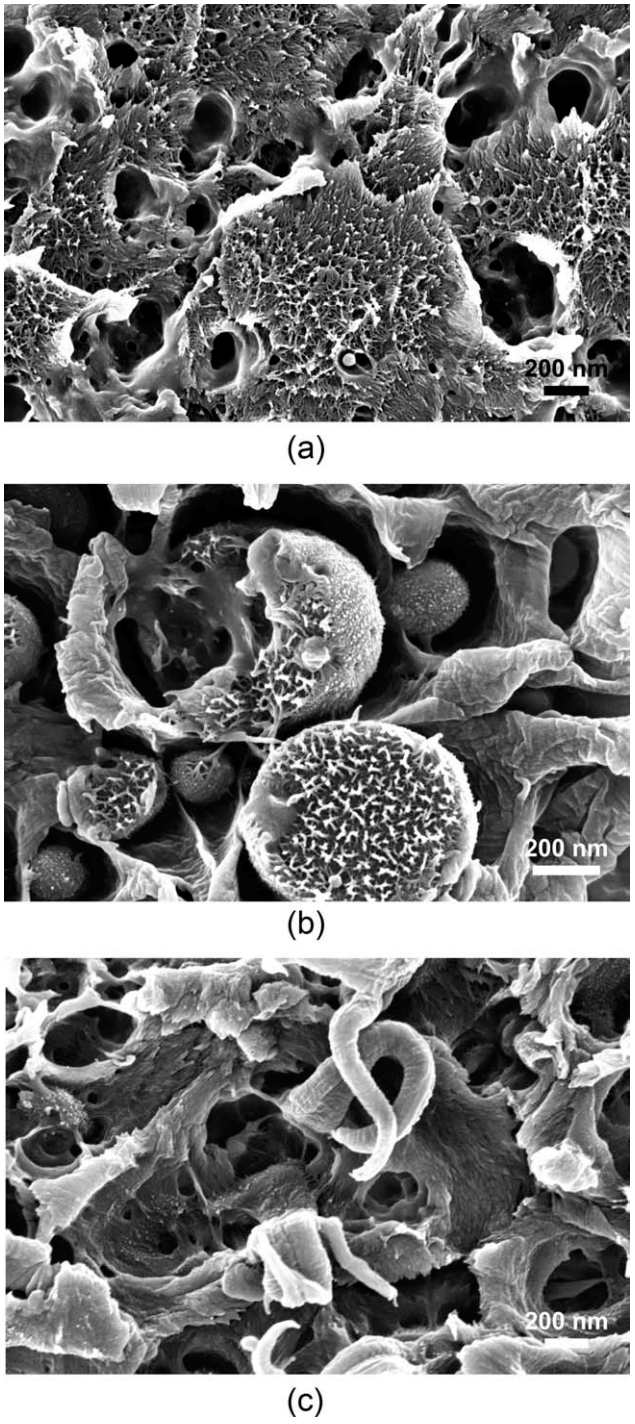

Figure 10 Scanning electron micrographs of the fracture surface of (a) neat ABS, (b) a 70% PA 6/30% ABS blend with 4% SANMA, and (c) a 30% PA 6/70% ABS blend with 4% SANMA. The acicular structures of ruptured and eventually relaxed craze fibrils are prominent in the surfaces of neat ABS [Fig. 10(a)] and disrupted ABS inclusions [Fig. 10(b)] of the compatibilized 70% PA 6/30% ABS blend.

deformation of the matrix [Fig. 9(f)]. An increasing SANMA concentration reduces the average size of the dispersed ABS phase and the amount of interfacial failure [Fig. 9(g,h)], but ductile failure of the matrix seems to be the dominant mechanism in the blends with a PA 6 matrix.

DISCUSSION

Melt flow properties

The rheological data reveal that reactive compatibilization strongly increases the shear viscosity within the entire range of shear rates investigated due to the formation of high-molecular weight graft copolymers. The increase in viscosity is more pronounced when PA 6 forms the matrix phase (cf. Fig. 3). This phenomenon is caused by the formation of very small highly compatibilized ABS and SAN inclusions, which strongly increase the viscosity of the PA 6 matrix. The extrudate swell data show that the reversible part of the deformation is also affected by compatibilization. Low degrees of compatibilization promote elastic recovery having passed the die, because coarse dispersed particles have larger capillary numbers than smaller ones hence they experience larger stretch ratios. On the contrary, in the elongation and subsequent recovery experiments of Refs. 24–26, the macroscopic elongation rate was kept constant. Such a strain-rate driven flow does not necessarily lead to a lower capillary number with rising SANMA concentrations. For example, the viscosity of the blends investigated in Refs. 24–26 increased with SANMA concentration, and the recovered stretch after elongation with a constant strain rate increased with SANMA concentration. This result emphasizes the difference between pressure-driven and strain-rate driven flows. Although reactive compatibilization increases the viscosity at low shear rates, the processing properties are only moderately altered, because at high shear rates, only moderate differences between the blend and the pristine components exist. The increase of viscosity is mostly pronounced in PA 6-based blends at high SANMA concentrations.

Mechanical properties

The analysis of the mechanical experiments reveals that blending of PA 6 with an ABS copolymer of low rubber content reduces the modulus of elasticity E below that of the neat constituents independent of the nature of the continuous phase and the degree of compatibilization. Because neither blending nor compatibilization impairs the crystallinity of PA 6 domains, the low tensile modulus is assumed to arise from the low bonding strength of the dispersed particles to the particular matrix polymer. This may result in particle detachment either by high stresses in certain parts of the interfaces even at low strains due to stress concentration or differential shrinkage

already during cooling—see Ref. 43—for example, in PA 6/ABS 30/70 blends. Voids reduce the effective cross-section and thus the modulus if created at low strains. When the dispersed ABS particles are sufficiently bonded to the matrix, crazes will be initiated in the inclusions before detachment from the continuous phase, PA 6, sets on. This becomes evident from SEM at SANMA concentrations greater than about 2 wt %. However, the occurrence of crazing is not accompanied by a significant increase in toughness as might be expected. The marginal contribution of crazing to the energy dissipation at impact loading, thus to the toughness of the blend, is most likely due to the low rubber content in the deployed ABS. The restriction to low rubber concentrations turned out to be necessary to be able to perform elongational experiments.[24–26]

The influence of reactive compatibilization on the fracture behavior is much more pronounced than on the modulus of elasticity. Generally, the properties of the matrix phase dominate the behavior of polymer blends with a droplet morphology. Furthermore, the blend properties are usually inferior to the pristine components because of interfacial failure in the blends. Increasing the concentration of SANMA enhances the fracture properties. This is clearly seen for the specific work to break and the impact strength. The increase of strength is most significant when PA 6 forms the matrix. This effect can be explained by the formation of graft polymers comprising SAN and PA 6 branches, which compatibilize the two phases and also form tiny SAN inclusions in the PA 6 matrix. As in the case of a PA 6 matrix, interfacial failure of uncompatibilized blends strongly decreases the fracture mechanical properties the improvement of the interfacial adhesion via reactive compatibilization should have a strong effect. Whether the tiny, micelle-like highly compatibilized SAN/ABS domains [see the domain marked by an arrow in Figure 2(e) or the matrix phase in Figure 2(i)], which modify the PA 6 matrix of the blends, have any additional impact on the toughness was not investigated. Because the matrix material determines the overall fracture mechanical behavior, reactive compatibilization can only moderately improve the end-use properties of blends based on brittle ABS. Albeit the investigations on blends with a disperse morphology have clearly revealed the effects of reactive compatibilization, a co-continuous morphology would yield optimal properties and would thus be the preferred structure for technical applications.

An interesting conclusion can be drawn from the analysis of the fatigue crack propagation experiments. If ABS forms the matrix, an increasing SANMA concentration generally increases the resistance to crack propagation, in particular for SANMA concentrations of 1–2 wt %. This effect is caused by the compatibilizing reaction, which enhances interfacial adhesion and consequently reduces interfacial failure. An unexpected result observed for blends with a PA 6 matrix is the enhancement of impact strength with increasing SANMA concentrations, whereas their fatigue crack propagation resistance tends to decrease. A source of this phenomenon might be the extension of the deformation zone ahead of the crack tip, which is much more confined in fatigue tests than in impact tests. In PA 6-based blends with tiny ABS and SAN inclusions, ductile failure dominates fatigue crack growth. Therefore, the dependence of da/dN on ΔK differs for blends with 70% PA 6 and for neat PA 6.

CONCLUSIONS

Reactive compatibilization strongly influences the properties of blends of PA 6 and an ABS copolymer in the solid and in the melt state. Morphological investigations revealed that reactive compatibilization using a specific SANMA terpolymer reduces the coalescence of domains of the dispersed phase during melt blending, that is, the coalescence of domains at short times. Hence the average size of PA 6 and ABS inclusions, respectively, is decreased. Furthermore, reactive compatibilization increases the shear viscosity and strongly influences the extrudate swell of PA 6/ABS blends in the melt. Because the capillary number in shear and elongation is a function of the mean drop radius, the decrease of the average size of the domains with SANMA concentration must be taken into account when predicting the flow properties of compatibilized PA 6/ABS blends. The measurements of the extrudate swell reveal that this effect is highly relevant for pressure-driven flows.

The Young's modulus is only moderately influenced by the formation of SAN-*graft*-PA 6 copolymers in PA 6/ABS blends. Specific work to break and impact strength increase with rising SANMA concentrations but do not exceed the properties of the pristine components. This result shows that reactive compatibilization enhances the mechanical performance of PA 6/ABS blends compared to uncompatibilized blends by improving the interfacial adhesion between the PA 6 and the ABS phase. This effect is strongly pronounced and exceeds the influence of the particle size on the mechanical properties. The resistance to fatigue crack propagation of blends with an ABS matrix is improved by the addition of 1–2 wt % SANMA. In the blends with a PA 6 matrix, ductile failure of the PA 6 matrix dominates the fatigue crack growth properties. A SANMA concentration in the order of 2 wt % yields an optimal

combination of morphological, mechanical, and rheological properties.

We are grateful to Professor Clive Bucknall for a critical reading of the manuscript. We thank Mr. Alexander Brückner for fatigue crack propagation experiments, Ms. Anne Lang (University of Bayreuth) for scanning electron microscopy investigations, Mr. Stefan Forster for mechanical testing, Dr. J. Mertes (both BASF SE, Ludwigshafen) for DSC measurements, Mr. Thomas Cüper (Bayer MaterialScience AG, Leverkusen) for rheological experiments, and Mr. A. Rozanski (Centre of Molecular and Macromolecular Studies, Lodz) for experimental support.

References

1. Utracki, L. A. Polymer Alloys and Blends: Thermodynamics and Rheology; Hanser: Munich, 1989.
2. Utracki, L. A. Commercial Polymer Blends; Chapman & Hall: London, 1998.
3. Paul, D. R.; Bucknall, C. B., Eds. Polymer Blends, Vol.1: Formulation and Vol.2: Performance; Wiley: New York, 2000.
4. Weber, M. Macromol Symp 2001, 163, 235.
5. Weber, M. Macromol Symp 2002, 181, 189.
6. van Duin, M.; Machado, A. V.; Covas, J. Macromol Symp 2001, 170, 29.
7. Weber, M.; Heckmann, W.; Goeldel, A. Macromol Symp 2006, 233, 1.
8. Jafari, S. H.; Pötschke, P.; Stephan, M.; Warth, H.; Alberts, H. Polymer 2002, 43, 6985.
9. Jafari, S. H.; Pötschke, P.; Stephan, M.; Pompe, G.; Warth, H.; Alberts, H. J Appl Polym Sci 2002, 84, 2753.
10. Lee, C. W.; Ryu, S. H.; Kim, H. S. J Appl Polym Sci 1997, 64, 1595.
11. Kudva, R. A.; Keskkula, H.; Paul, D. R. Polymer 2000, 41, 225.
12. Takeda, Y.; Paul, D. R. J Polym Sci Part B: Polym Phys 1992, 30, 1273.
13. Majumdar, B.; Paul, D. R.; Oshinski, A. J. Polymer 1997, 38, 1787.
14. Kitayama, N.; Keskkula, H.; Paul, D. R. Polymer 2001, 42, 3751.
15. Majumdar, B.; Keskkula, H.; Paul, D. R. Polymer 1994, 35, 3164.
16. Majumdar, B.; Keskkula, H.; Paul, D. R., Polymer 1994, 35, 5453.
17. Pressly, T. G.; Keskkula, H.; Paul, D. R. Polymer 2001, 42, 3043.
18. Araújo, E. M.; Hage E., Jr.; Carvalho, A. J. F. J Appl Polym Sci 2003, 87, 842.
19. Araújo, E. M.; Hage, E., Jr.; Carvalho, A. J. F. J Appl Polym Sci 2003, 90, 2643.
20. Araújo, E. M.; Hage, E., Jr.; Carvalho, A. J. F. J Mater Sci 2005, 40, 4239.
21. Steenbrink, A. C.; Janik, H.; Gaymans, R. J. J Mater Sci 1997, 32, 5505.
22. Handge, U. A.; Sailer, C.; Steininger, H.; Weber, M.; Scholtyssek, St.; Seydewitz, V. Michler, G. H. J Appl Polym Sci 2009, 112, 1658.
23. Handge, U. A.; Sailer, C.; Steininger, H.; Weber, M.; Scholtyssek, St.; Seydewitz, V.; Michler, G. H. J Appl Polym Sci 2010, 115, 2529.
24. Sailer, C.; Handge, U. A. Macromolecules 2007, 40, 2019.
25. Sailer, C.; Handge, U. A. Macromol Symp 2007, 254, 217.
26. Sailer, C.; Handge, U. A. Macromolecules 2008, 41, 4258.
27. Sailer, C.; Weber, M.; Steininger, H.; Handge, U. A. Rheol Acta 2009, 48, 579.
28. Triacca, V. J.; Ziaee, S.; Barlow, J. W.; Keskkula, H.; Paul, D. R. Polymer 1991, 32, 1401.
29. Altstädt, V. Adv Polym Sci 2005, 188, 105.
30. Castellani, L.; Rink, M. In Fracture Mechanics Testing Methods for Polymers, Adhesives and Composites; Moore, D. R., Pavan, A., Williams, J. G., Eds.; Elsevier: Amsterdam, 2001; p 91–116; ISBN: 0-08-043689-7.
31. Saxena, A.; Hudak, S. J. Int J Fract 1978, 14, 453.
32. Münstedt, H. Polym Eng Sci 1981, 21, 259.
33. Gramespacher, H.; Meissner, J. J Rheol 1997, 41, 27.
34. Handge, U. A.; Pötschke, P. J Rheol 2004, 47, 969; Erratum J Rheol 2005, 48, 1153.
35. Handge, U. A.; Okamoto, K.; Münstedt, H. Rheol Acta 2007, 46, 1197.
36. Stary, Z.; Musialek, M.; Münstedt, H. Macromol Mater Eng 2011, 296, 414.
37. Stary, Z.; Machui, F.; Münstedt, H. Polymer 2010, 51, 3744.
38. Paris, P.; Erdogan, F. J Basic Eng Trans ASME 1963, 528.
39. Ruckdäschel, H.; Fischer, F.; Altstädt, V.; Müller, A. H. E. J Solid Mech Mater Eng 2008, 2, 417.
40. Karger-Kocsis, J.; Friedrich, K. Composites 1988, 19, 105.
41. Bellemare, S. C.; Bureau, M. N.; Denault, J.; Dickson, J. I. Polym Compos 2004, 25, 433.
42. Bucknall, C. B. J Polym Sci Polym Phys 2007, 45, 1399.
43. Bucknall, C. B.; Ayre, D. S.; Dijkstra, D. J. Polymer 2000, 41, 5937.